

# DATA-DRIVEN SPECTRAL ANALYSIS THROUGH PSEUDO-RESOLVENT KOOPMAN OPERATOR IN DYNAMICAL SYSTEMS

Yuanchao Xu<sup>1\*†</sup> Itsushi Sakata<sup>2†</sup> Isao Ishikawa<sup>1</sup>

<sup>1</sup> Center for Science Adventure and Collaborative Research Advancement (SACRA)

Graduate School of Science, Kyoto University

<sup>2</sup> RIKEN Center for Advanced Intelligence Project

## ABSTRACT

We present a data-driven method for spectral analysis of the Koopman operator based on direct construction of the pseudo-resolvent from time-series data. Finite-dimensional approximations of the Koopman operator, such as those obtained from Extended Dynamic Mode Decomposition, are known to suffer from spectral pollution. To address this issue, we construct the pseudo-resolvent operator using the Sherman-Morrison-Woodbury identity whose norm serves as a spectral indicator, and pseudoeigenfunctions are extracted as directions of maximal amplification. We establish convergence of the approximate spectrum to the true spectrum in the Hausdorff metric for isolated eigenvalues, with preservation of algebraic multiplicities, and derive error bounds for eigenvalue approximation. Numerical experiments on pendulum, Lorenz, and coupled oscillator systems demonstrate that the method effectively suppresses spectral pollution and resolves closely spaced spectral components.

## 1 Introduction

The study of nonlinear dynamical systems is central to many scientific and engineering problems [1, 2, 15, 27, 30, 31]. Traditionally, their analysis relies on first-principles models together with tools such as phase-space geometry [27], perturbation methods [14] for weak nonlinearities, and direct numerical simulation. These approaches have delivered deep insight, but they can be difficult to use when an accurate governing model is unavailable, when model parameters are uncertain, or when the goal is to infer global dynamical features from observations rather than describe local behavior near equilibria [10, 11]. Meanwhile, modern experiments and simulations increasingly produce large amounts of time-series measurements, which has attracted growing interest in data-driven methods that aim to characterize dynamical behavior directly from data.

A natural perspective for data-driven analysis is to focus on the evolution of observable quantities rather than the underlying state variables. In many applications, one does not have direct access to the full state of a system but instead observations of the state, e.g., temperatures, velocities, concentrations, or other quantities of interest. The Koopman operator provides a mathematical framework for this viewpoint; more specifically, it describes how observables evolve in time by composing them with the flow map of the dynamical system [18, 19, 23]. Although the underlying dynamics may be nonlinear, the Koopman operator acts linearly on the space of observables, enabling spectral analysis to reveal dynamical features such as oscillation frequencies, growth and decay rates, and coherent structures. Dynamic Mode Decomposition (DMD) [33] and its extension, Extended Dynamic Mode Decomposition (EDMD) [34], provide practical algorithms for approximating the Koopman operator and its spectral properties directly from time-series data, and theoretical foundations have established convergence of these approximations under appropriate conditions [5, 7, 13, 17, 20, 36].

Despite these convergence guarantees, a fundamental difficulty arises when extracting spectral information from finite-dimensional approximations: the phenomenon of spectral pollution [5]. The approximating matrix is finite-dimensional and therefore possesses a discrete spectrum, whereas the true Koopman operator includes continuous

---

\*Corresponding Authors. Email to: xu.yuanchao.3a@kyoto-u.ac.jp

†Equal Contributions.

spectral components (see, e.g., [22]). Consequently, computed eigenvalues may include spurious points that do not correspond to any part of the true spectrum. In other words, these are drawbacks of the finite-dimensional truncation rather than intrinsic dynamical features. Conversely, true spectral points may be missed entirely if they are not well-represented by the chosen dictionary. This problem is not merely a matter of insufficient data or dictionary size; it is a structural consequence of approximating an infinite-dimensional operator by finite-dimensional matrices.

To address spectral pollution, Residual Dynamic Mode Decomposition [5] was introduced to validate candidate eigenvalues by computing residuals of approximate eigenfunctions. The key insight is that small residuals provide a certificate that a computed eigenvalue lies near the true spectrum, while large residuals indicate potential spectral pollution. This approach achieves rigorous convergence to spectral measures of the Koopman operator and provides a rigorous framework for spectral computation. However, its implementation requires careful estimation of approximation errors associated with finite-dimensional projections, as these errors can be sensitive to the choice of dictionary and to the underlying spectral structure.

In this paper, we explore an alternative approach based on direct construction of the pseudo-resolvent operator from data [9, 12, 14, 32]. The resolvent encodes complete spectral information through its operator norm, which becomes large precisely when the spectral parameter approaches the spectrum. We show that the Sherman-Morrison-Woodbury identity enables efficient computation of the pseudo-resolvent directly from data matrices, and we extract pseudoeigenfunctions as directions of maximal amplification under this operator. We establish convergence of the approximate spectrum to the true spectrum in the Hausdorff metric with preservation of algebraic multiplicities, and derive error bounds for eigenvalue approximations [4, 14, 25]. Numerical experiments on pendulum, Lorenz, and coupled oscillator systems demonstrate the effectiveness of the method in suppressing spectral pollution and resolving closely spaced spectral components.

The remainder of this paper is organized as follows. Section 2 reviews the necessary background on Koopman operators, resolvents, and pseudo-resolvents. Section 3 presents the data-driven construction of the pseudo-resolvent matrix. Section 4 develops the convergence theory, including Hausdorff convergence of spectra and conditions for multiplicity preservation. Section 5 derives error bounds controlled by residual quantities. Section 6 presents numerical experiments on pendulum, Lorenz, and coupled oscillator systems. Section 7 concludes with a discussion of the method’s scope and directions for future work.

## 2 Preliminaries

### 2.1 Koopman Operator

The Koopman operator is a cornerstone of modern dynamical systems theory, offering a linear framework to study the evolution of nonlinear systems. Consider a dynamical system defined on the state space  $\mathcal{M}$  equipped with a measure  $\mu$  (which is not necessarily invariant), and let  $T : \mathcal{M} \rightarrow \mathcal{M}$  be the transformation map. The bounded Koopman operator  $\mathcal{K}$  associated with  $T$  acts on the space of square-integrable functions  $\mathcal{F} := L^2(\mathcal{M}, \mu)$ . The inner product is defined by  $\langle f, g \rangle := \int_{\mathcal{M}} \bar{f}g \, d\mu$ , and the operator is given by

$$\mathcal{K}f(x) = f(T(x)), \quad \forall f \in \mathcal{F}, \quad \forall x \in \mathcal{M}.$$

In our framework, the analysis and convergence results are primarily developed for this discrete-time Koopman operator  $\mathcal{K}$ .

It is important to note that many dynamical systems are naturally continuous in time. In such cases, the dynamics are described by a flow  $\{T_t\}_{t \geq 0}$  and the corresponding Koopman operator generalizes to a one-parameter semigroup  $\{\mathcal{K}^t\}_{t \geq 0}$  defined by

$$\mathcal{K}^t f(x) = f(T_t(x)), \quad \forall f \in \mathcal{F}, \quad t \geq 0.$$

Under standard assumptions, e.g.,  $C_0$  semigroup [8, 26], this Koopman semigroup has a closed and densely defined generator  $\mathcal{A}$  such that  $\mathcal{K}^t = e^{t\mathcal{A}}$  for  $t \geq 0$ . In our study, the discrete-time operator  $\mathcal{K}$  is viewed as the embedded system obtained by sampling the continuous-time flow at unit time  $t = 1$ , i.e.,

$$\mathcal{K} = \mathcal{K}^1. \tag{1}$$

This relationship allows us to leverage the rich theoretical framework of discrete approximation for convergence analysis while establishing a direct connection to the continuous-time dynamics. In the pendulum example of Section 6.1, Figures 1 and 2 are based on the discrete operator  $\mathcal{K}$  (or its finite-dimensional approximation), whereas Figure 3 investigates the continuous-time generator. This dual perspective ensures that our discrete framework not only rigorously captures the spectral properties of  $\mathcal{K}$  but also provides a pathway to understand the continuous-time dynamics via this embedding as in Eq. (1).

The power of the Koopman operator lies in its ability to linearize nonlinear dynamics: even when  $T$  is highly nonlinear,  $\mathcal{K}$  induces a linear evolution on  $\mathcal{F}$ . Spectral analysis of  $\mathcal{K}$  through its eigenvalues, eigenfunctions, and invariant subspaces reveals critical dynamical properties such as periodicity, mixing, and chaos. For a contractive  $\mathcal{K}$ , its spectrum  $\sigma(\mathcal{K})$  lies within the closed unit disk. When considering the continuous-time generator  $\mathcal{A}$ , the spectrum is typically confined to the left half-plane,  $\text{Re}(z) \leq 0$ , which reflects dissipative dynamics.

Moreover, under appropriate conditions, the spectral mapping theorem provides a rigorous link between the spectrum of the generator  $\mathcal{A}$  and that of the semigroup  $\{\mathcal{K}^t\}_{t \geq 0}$ . In particular, when  $\mathcal{K}^t = e^{t\mathcal{A}}$  and  $t = 1$ , the theorem asserts that

$$\sigma(\mathcal{K}) = \{e^\lambda : \lambda \in \sigma(\mathcal{A})\},$$

provided that  $\mathcal{K}$  is bounded and  $\mathcal{A}$  generates a strongly continuous semigroup. This relationship not only validates the discrete-time framework (where  $\mathcal{K} = \mathcal{K}^1$ ) as an embedded representation of the continuous-time dynamics but also enables the computation of the generator's spectral properties via the more accessible spectrum of  $\mathcal{K}$ .

In practice, the Koopman operator is particularly valuable in data-driven analysis [3, 5, 13, 17, 21, 23, 24, 34, 36, 37], as it allows one to approximate  $\mathcal{K}$  directly from time-series data without requiring an explicit model for  $T$ . This approach has been successfully applied in diverse fields such as fluid dynamics, neuroscience, and statistical mechanics, where the evolution of observables is often more accessible than tracking individual trajectories.

## 2.2 Resolvent and Pseudo-Resolvent Operator

The resolvent is a fundamental concept in operator theory, particularly for linear operators on the space  $\mathcal{F}$ . For a linear operator  $\mathcal{A}$  (possibly unbounded) defined on a dense subspace of  $\mathcal{F}$ , its spectrum  $\sigma(\mathcal{A})$  consists of all complex numbers  $z$  for which  $zI - \mathcal{A}$  (with  $I$  the identity operator) is not invertible. The resolvent set  $\rho(\mathcal{A})$  is the complement of  $\sigma(\mathcal{A})$  in  $\mathbb{C}$ , i.e. those  $z$  where  $zI - \mathcal{A}$  has a bounded inverse. The resolvent of  $\mathcal{A}$  at  $z \in \rho(\mathcal{A})$  is the operator  $\mathcal{R}(z, \mathcal{A}) = (zI - \mathcal{A})^{-1}$ , which maps  $\mathcal{F}$  into the domain  $\mathcal{D}(\mathcal{A})$  of  $\mathcal{A}$ . This operator  $\mathcal{R}(z, \mathcal{A})$  is bounded and provides a way to "resolve" the equation  $(zI - \mathcal{A})f = g$  by giving  $f = \mathcal{R}(z, \mathcal{A})g$  whenever  $z$  lies outside the spectrum. The resolvent  $\mathcal{R}(z, \mathcal{A})$  has several useful properties. It is an analytic (holomorphic) function of  $z$  on  $\rho(\mathcal{A})$ , often expressible via a Neumann series when  $|z|$  is large or  $z$  is near some  $z_0 \in \rho(\mathcal{A})$ . It also satisfies the *first resolvent identity*: for any  $z, \mu \in \rho(\mathcal{A})$ ,

$$\mathcal{R}(z, \mathcal{A}) - \mathcal{R}(\mu, \mathcal{A}) = (\mu - z) \mathcal{R}(z, \mathcal{A}) \mathcal{R}(\mu, \mathcal{A}),$$

which can be verified by manipulating  $(zI - \mathcal{A})^{-1} - (\mu I - \mathcal{A})^{-1}$  and factoring out  $(\mu - z)$ . This identity is central to understanding the continuity and differentiability of  $\mathcal{R}(z, \mathcal{A})$  and links  $\mathcal{R}(z, \mathcal{A})$  to the spectral properties of  $\mathcal{A}$ . For instance, if  $\mathcal{A} = \mathcal{K}$  is the Koopman operator on  $\mathcal{F}$  and  $\mathcal{K}$  is contractive, then the spectrum  $\sigma(\mathcal{K})$  lies inside the unit disk, and the resolvent  $\mathcal{R}(z, \mathcal{K})$  exists (is bounded) for all  $|z| > 1$ . This provides a window into the frequencies or growth/decay rates of the dynamical system underlying  $\mathcal{K}$ .

A generalization of the resolvent operator is the pseudo-resolvent, which extends the framework beyond cases where a well-defined generating operator exists. A family of operators  $\{\mathcal{R}(z)\}_{z \in \Omega}$ , where  $\Omega$  is a subset of the complex plane  $\mathbb{C}$ , is called a pseudo-resolvent if it satisfies the *first resolvent identity* [8, 14]:

$$\mathcal{R}(z) - \mathcal{R}(\mu) = (\mu - z) \mathcal{R}(z) \mathcal{R}(\mu), \quad \forall z, \mu \in \Omega.$$

This definition does not assume the existence of an operator  $\mathcal{A}$  such that  $\mathcal{R}(z) = (zI - \mathcal{A})^{-1}$ . When such an operator exists, the pseudo-resolvent is said to be representable.

Pseudo-resolvents maintain many important properties of standard resolvents, including analyticity on their domain of definition. The domain of a pseudo-resolvent, analogous to the resolvent set, consists of points  $z \in \mathbb{C}$  where  $\mathcal{R}(z)$  exists as a bounded operator. The spectrum associated with a pseudo-resolvent can still be defined as the complement of this domain in  $\mathbb{C}$ .

The flexibility of pseudo-resolvents makes them particularly valuable in data-driven contexts, where the underlying operator might not be explicitly available or might not exist in the classical sense. In such settings, constructing a family of operators that satisfies the resolvent identity often provides sufficient analytical power, even without an explicit representation in terms of a generating operator. This approach is especially relevant for complex dynamical systems where complete knowledge of the system's operator or generator may be unavailable, but data-driven approximations can still capture essential spectral characteristics of the dynamics.

## 3 A Data-Driven Computational Approach for Pseudo-Resolvent Estimation

Recall that the EDMD-approximated Koopman operator (semigroup) matrix  $\mathbf{K}_N$  [34] and generator matrix  $\mathbf{A}_N$  [17] are:

$$\mathbf{K}_N = \Psi_X^\dagger \Psi_Y \quad \mathbf{A}_N = \Psi_X^\dagger \Psi_X', \quad (2)$$

where  $\Psi_X, \Psi_Y \in \mathbb{C}^{M \times N}$  are  $N$  basis evaluations at  $M$  data points,  $\Psi'_X = (\Psi_Y - \Psi_X)/\Delta t$  and  $\Psi_X^\dagger$  is the pseudoinverse of  $\Psi_X$ .

**Remark 3.1.** Alternatively, one can also apply the Itô formula to compute each element in the matrix  $\Psi'_X$  if the system is stochastic. See [17, 36] for more details.

The **Sherman-Morrison-Woodbury (SMW)** [35] identity is the following:

$$(A + UV)^{-1} = A^{-1} - A^{-1}U(I + VA^{-1}U)^{-1}VA^{-1} \quad (3)$$

For each  $z \in \mathbb{C}$ , apply Eq. (3) to the pseudo-resolvent matrix  $(zI - \Psi_X^\dagger \Psi_Y)^{-1}$  with  $A = zI, U = -\Psi_X^\dagger, V = \Psi_Y$ , we have

$$\mathbf{R}_N(z) := \frac{1}{z}I + \frac{1}{z^2}\Psi_X^\dagger(I - \frac{1}{z}\Psi_Y\Psi_X^\dagger)^{-1}\Psi_Y. \quad (4)$$

Note that the construction of pseudo-resolvent matrix  $\mathbf{R}_N(z)$  is equivalent to the resolvent matrix  $\mathbf{R}(z, \mathbf{K}_N)$  by Eq. (2); specifically,

$$\mathbf{R}_N(z) = (zI - \Psi_X^\dagger \Psi_Y)^{-1} = (zI - \mathbf{K}_N)^{-1} = \mathbf{R}(z, \mathbf{K}_N) \quad (5)$$

Thus, by Eq. (5), we can verify the matrix identity for difference of inverses in the following:

$$\begin{aligned} \mathbf{R}_N(z) - \mathbf{R}_N(w) &= (zI - \mathbf{K}_N)^{-1} - (wI - \mathbf{K}_N)^{-1} \\ &= (zI - \mathbf{K}_N)^{-1} [(wI - \mathbf{K}_N) - (zI - \mathbf{K}_N)] (wI - \mathbf{K}_N)^{-1} \\ &= (w - z)\mathbf{R}_N(z)\mathbf{R}_N(w) \end{aligned}$$

Analogously, the corresponding pseudo-resolvent matrix  $(zI - \Psi_X^\dagger \Psi'_X)^{-1}$  for a generator study in a continuous-time setting is given by:

$$\begin{aligned} \mathbf{R}_N(z) &:= \frac{1}{z}I + \frac{1}{z^2}\Psi_X^\dagger(I - \frac{1}{z}\Psi'_X\Psi_X^\dagger)^{-1}\Psi'_X \\ &= (zI - \Psi_X^\dagger \Psi'_X)^{-1} = (zI - \mathbf{A}_N)^{-1} = \mathbf{R}(z, \mathbf{A}_N). \end{aligned} \quad (6)$$

**Remark 3.2.** In this paper, we will use the notation  $\mathbf{R}_N(z)$  for both  $\mathbf{R}(z, \mathbf{K}_N)$  and  $\mathbf{R}(z, \mathbf{A}_N)$ , depending on the context of the discussion.

The matrix approximation  $\mathbf{R}_N(z)$  can be viewed as a pseudo-resolvent operator approximation since this construction is entirely data-driven, working directly with the data matrices rather than requiring an explicit construction of the matrix representation  $\mathbf{K}_N$  of Koopman operator approximation  $\mathcal{K}_N$  first. Simultaneously, due to the mathematical equivalence established through the Sherman-Morrison-Woodbury formula, this matrix approximation  $\mathbf{R}_N(z)$  is mathematically equivalent to a standard resolvent operator approximation  $\mathbf{R}(z, \mathbf{K}_N) = (zI - \mathbf{K}_N)^{-1}$ . This equivalence ensures that all the theoretical results proven in Section 4 of the paper—including norm resolvent convergence property, spectral boundary stability, and Hausdorff distance convergence—remain valid and applicable. In this interpretation, we can leverage the theoretical foundations developed for standard resolvent operators while maintaining the practical benefits of a directly data-driven construction that aligns with pseudo-resolvent formulations.

**Remark 3.3.** Residual DMD [5] and the resolvent-based approach developed here are closely related in that both aim to mitigate spectral pollution by accessing pseudospectral information of the Koopman operator. Conceptually, these are two complementary viewpoints of the same underlying quantity: the  $\varepsilon$ -pseudospectrum can be characterized either through a residual condition (existence of a unit-norm vector with small defect) or through resolvent amplification. ResDMD adopts the residual viewpoint and provides *a posteriori* validation for candidate spectral points by computing minimal residuals of approximate eigenfunctions (and related adjoint information). In contrast, our method constructs a data-driven approximation of the (pseudo-)resolvent directly and extracts pseudospectral features through its norm and dominant amplification directions. From a practical standpoint, residual-based certification can be advantageous when the goal is to validate a small number of candidate eigenpairs, whereas resolvent-based probing naturally produces global pseudospectral contour plots and associated pseudomodes, at the cost of evaluating the resolvent over a set of spectral parameters.

## 4 Convergence Analysis of Spectrum

**Definition 4.1.** Denote by  $\sigma(\mathcal{K})$  the spectrum of the bounded Koopman operator  $\mathcal{K}$ . Let  $\mathcal{K}_N$  be a sequence of finite-dimensional discretized operators approximating  $\mathcal{K}$  resulting from the discretization by Galerkin approximation [20, 34]. The resolvent operator  $\mathcal{R}(z)$  is defined as:

$$\mathcal{R}(z) := \mathcal{R}(z, \mathcal{K}) = (zI - \mathcal{K})^{-1},$$

for  $z \in \rho(\mathcal{K})$ , where  $\rho(\mathcal{K})$  is the resolvent set of  $\mathcal{K}$  [14].

For the finite-dimensional approximation  $\mathcal{K}_N$ , we define a data-driven approximation of the pseudo-resolvent operator  $\mathcal{R}_N(z)$  whose matrix representation in the chosen dictionary is given by the large data limit  $\lim_{M \rightarrow \infty} \mathbf{R}_N(z)$  as formulated in Eq. (4). This approximation is valid for all  $z \in \rho(\mathcal{K}_N)$ , where  $\rho(\mathcal{K}_N)$  is the resolvent set of  $\mathcal{K}_N$ .

Notice that the convergence of  $\lim_{M \rightarrow \infty} \mathbf{R}_N(z)$  in large data is guaranteed by examining its structure in Eq. (4). This expression can be expanded as a Neumann series where each term involves powers of the Koopman operator matrix. According to EDMD theory [20, 34], these matrices converge almost surely in the large data limit  $M \rightarrow \infty$ , where  $M$  represents the number of data points. Specifically, under appropriate sampling conditions, the empirical averages (i.e., the two Gram matrices formed by Galerkin approximation) in the EDMD procedure converge to their expected values by the Strong Law of Large Numbers (SLLN), ensuring that our pseudo-resolvent operator approximation  $\mathcal{R}_N(z)$  is well-defined and reliable for spectral analysis. Moreover, since  $\mathcal{K}$  is bounded,  $\mathcal{K}_N \rightarrow \mathcal{K}$  in strong operator topology as proved in [20, Theorem 3]. However, this does not imply the same convergence type for  $\mathcal{R}_N(z) \rightarrow \mathcal{R}(z)$ . It is only true under an extra condition, as we will discuss later.

Let  $\mathcal{R}_N(z)$  be the (finite dimensional) pseudo-resolvent operator whose matrix representation is given in Eq. (4). Due to Eq. (5), we know that

$$\mathcal{R}_N(z) = \mathcal{R}(z, \mathcal{K}_N) = (zI - \mathcal{K}_N)^{-1}.$$

**Assumption 4.2.** For any  $z \in \rho(\mathcal{K})$  there exists  $N(z)$  such that for all  $N > N(z)$ , we have  $z \in \rho(\mathcal{K}_N)$  and

$$\|\mathcal{R}_N(z)\| \leq M_z, \quad (7)$$

for some  $M_z < \infty$  independent of  $N$ .

Assumption 4.2 is usually called *stable convergence* [4, Chapter 3.4]. It acts as a stability condition that prevents ill-conditioning in the approximation process. Without such a condition, spectral approximation could produce spurious eigenvalues or fail to capture the true spectral properties of the original operator.

**Remark 4.3.** Recall *second resolvent identity* [8, 14]:  $\mathcal{R}(z) - \mathcal{R}_N(z) = \mathcal{R}_N(z)(\mathcal{K} - \mathcal{K}_N)\mathcal{R}(z)$ . By Eq. (7) and the *second resolvent identity*, we obtain a strong convergence for  $\mathcal{R}_N(z)$ , i.e., for each  $z \in U \subset \rho(\mathcal{K})$ , there exists  $N_z \in \mathbb{N}$  such that for  $N > N_z$ ,

$$\mathcal{R}_N(z)f \rightarrow \mathcal{R}(z)f, \quad \forall f \in \mathcal{F} \quad (8)$$

**Definition 4.4.** Let  $\lambda$  be an isolated eigenvalue of  $\mathcal{K}$  with algebraic multiplicity  $m_\lambda < \infty$  and  $\Gamma_\lambda$  be a closed Jordan curve around  $\lambda$  containing no other point of  $\sigma(\mathcal{K})$ . Define the spectral projection  $\mathcal{P}^\lambda, \mathcal{P}_N^\lambda$  associated with  $\lambda$  as:

$$\mathcal{P}^\lambda := \frac{1}{2\pi i} \int_{\Gamma_\lambda} \mathcal{R}(z) dz, \quad \mathcal{P}_N^\lambda := \frac{1}{2\pi i} \int_{\Gamma_\lambda} \mathcal{R}_N(z) dz.$$

Let  $\dim \mathcal{P}^\lambda \mathcal{F}, \dim \mathcal{P}_N^\lambda \mathcal{F}$  be the invariant subspace under the projection  $\mathcal{P}, \mathcal{P}_N$ .

**Assumption 4.5.** Let  $\lambda \in \sigma(\mathcal{K})$  be an isolated eigenvalue with algebraic multiplicity  $m_\lambda$ . Assume  $\dim \mathcal{P}_N^\lambda \mathcal{F} = \dim \mathcal{P}^\lambda \mathcal{F} = m_\lambda < \infty$  for all large  $N$ .

Assumption 4.5 is usually called *strongly stable convergence* [4, Chapter 5] which is essential for multiplicity preservation in the spectral convergence. This assumption is valid since we will later show that  $\dim \mathcal{P}_N^\lambda \mathcal{F} \geq m_\lambda$  whenever  $N$  is large enough in Corollary 4.9.

In the next Lemma 4.6, we will show a uniform bound for  $\mathcal{R}_N(z)$  over a compact subset of  $\rho(\mathcal{K})$ .

**Lemma 4.6.** Let  $U$  be a compact subset of the resolvent set  $\rho(\mathcal{K})$ . If Eq. (7) from Assumption 4.2 holds for all  $z \in U$ , then there exists  $N_U \in \mathbb{N}$  and a constant  $M_U < \infty$  such that

$$\sup_{z \in U, N > N_U} \|\mathcal{R}_N(z)\| \leq M_U.$$

*Proof.* Fix any  $z \in U$ . By Assumption 4.2, there exist  $N(z)$  and  $M_z < \infty$  such that for all  $N > N(z)$ ,  $z \in \rho(\mathcal{K}_N)$  and  $\|\mathcal{R}_N(z)\| \leq M_z$ . Define  $r_z := \frac{1}{2M_z}$ .

Now take any  $w \in \mathbb{C}$  with  $|w - z| < r_z$  and any  $N > N(z)$ . Using the *first resolvent identity*,

$$\mathcal{R}_N(w) - \mathcal{R}_N(z) = (z - w)\mathcal{R}_N(w)\mathcal{R}_N(z),$$

we obtain

$$\mathcal{R}_N(w)[I + (w - z)\mathcal{R}_N(z)] = \mathcal{R}_N(z).$$

Since  $\|(w - z)\mathcal{R}_N(z)\| \leq |w - z| \|\mathcal{R}_N(z)\| < \frac{1}{2}$ , the operator  $I + (w - z)\mathcal{R}_N(z)$  is invertible and

$$\|\mathcal{R}_N(w)\| \leq \frac{\|\mathcal{R}_N(z)\|}{1 - |w - z| \|\mathcal{R}_N(z)\|} \leq 2M_z.$$

Hence,

$$\sup_{w \in B(z, r_z), N > N(z)} \|\mathcal{R}_N(w)\| \leq 2M_z.$$

The collection  $\{B(z, r_z)\}_{z \in U}$  is an open cover of the compact set  $U$ , so we can extract a finite subcover  $\{B(z_j, r_{z_j})\}_{j=1}^J$ . Let

$$N_U := \max_{1 \leq j \leq J} N(z_j), \quad M_U := 2 \max_{1 \leq j \leq J} M_{z_j}.$$

Then for any  $N > N_U$  and any  $w \in U$ , there exists  $j$  with  $w \in B(z_j, r_{z_j})$  and therefore  $\|\mathcal{R}_N(w)\| \leq M_U$ . This proves the claim.  $\square$

**Lemma 4.7** ([4, Proposition 3.10]). Let  $\mathcal{P}$  and  $\mathcal{P}_N$  (for  $n \in \mathbb{N}$ ) be projections such that  $\mathcal{P}_N$  converges to  $\mathcal{P}$  pointwise, and let  $\dim \mathcal{P}\mathcal{F} < \infty$ . Then,  $\|(\mathcal{P} - \mathcal{P}_N)\mathcal{P}\| \rightarrow 0$  as  $N$  becomes sufficiently large, and for  $N$  large enough,  $\dim \mathcal{P}_N\mathcal{F} \geq \dim \mathcal{P}\mathcal{F}$ .

**Remark 4.8.** In many numerical methods, particularly those that rely on projecting infinite dimensional problems onto finite-dimensional subspaces (e.g. Galerkin approximation), Lemma 4.7 plays a fundamental role in ensuring stability and consistency of approximations. It guarantees that once  $\mathcal{P}_N$  converges strongly to a limiting projector  $\mathcal{P}$ , the dimension of the projected subspace  $\mathcal{P}_N\mathcal{F}$  cannot suddenly drop below  $\dim(\mathcal{P}\mathcal{F})$ . This means that the subspace capturing the ‘‘essential’’ part of the solution does not degenerate.

**Corollary 4.9.** Let  $\lambda$  be an isolated eigenvalue of  $\mathcal{K}$  with algebraic multiplicity  $m_\lambda$  and let  $\Gamma_\lambda$  be the isolating contour in Definition 4.4. Suppose Eq. (7) in Assumption 4.2 holds for all  $z \in \Gamma_\lambda$ . Then, for  $N$  sufficiently large,

$$\dim(\mathcal{P}_N^\lambda \mathcal{F}) \geq \dim(\mathcal{P}^\lambda \mathcal{F}) = m_\lambda.$$

*Proof.* Fix  $f \in \mathcal{F}$ . By Definition 4.4,

$$(\mathcal{P}_N^\lambda - \mathcal{P}^\lambda)f = \frac{1}{2\pi i} \int_{\Gamma_\lambda} (\mathcal{R}_N(z) - \mathcal{R}(z))f dz.$$

For each  $z \in \Gamma_\lambda$ , Eq. (8) implies  $\mathcal{R}_N(z)f \rightarrow \mathcal{R}(z)f$  as  $N \rightarrow \infty$ . Moreover, Lemma 4.6 (applied to  $U = \Gamma_\lambda$ ) yields constants  $N_\Gamma$  and  $M_\Gamma$  such that

$$\sup_{z \in \Gamma_\lambda, N > N_\Gamma} \|\mathcal{R}_N(z)\| \leq M_\Gamma.$$

Hence, for any  $z, w \in \Gamma_\lambda$  and  $N > N_\Gamma$ , the first resolvent identity gives

$$\|\mathcal{R}_N(z)f - \mathcal{R}_N(w)f\| \leq |z - w| \|\mathcal{R}_N(z)\| \|\mathcal{R}_N(w)\| \|f\| \leq |z - w| M_\Gamma^2 \|f\|.$$

Thus  $\{z \mapsto \mathcal{R}_N(z)f\}_{N > N_\Gamma}$  is equicontinuous and uniformly bounded on the compact set  $\Gamma_\lambda$ . Since the pointwise limit  $z \mapsto \mathcal{R}(z)f$  is continuous, an Arzelà–Ascoli argument [6] implies the convergence is uniform on  $\Gamma_\lambda$ , i.e.,

$$\sup_{z \in \Gamma_\lambda} \|(\mathcal{R}_N(z) - \mathcal{R}(z))f\| \rightarrow 0.$$

Therefore,

$$\|(\mathcal{P}_N^\lambda - \mathcal{P}^\lambda)f\| \leq \frac{|\Gamma_\lambda|}{2\pi} \sup_{z \in \Gamma_\lambda} \|(\mathcal{R}_N(z) - \mathcal{R}(z))f\| \rightarrow 0,$$

so  $\mathcal{P}_N^\lambda \rightarrow \mathcal{P}^\lambda$  pointwise. Applying Lemma 4.7 yields  $\dim(\mathcal{P}_N^\lambda \mathcal{F}) \geq \dim(\mathcal{P}^\lambda \mathcal{F})$  for  $N$  large enough.  $\square$

**Theorem 4.10.** Let  $\lambda$  be an isolated eigenvalue of  $\mathcal{K}$  with finite algebraic multiplicity  $m$ . Let  $\Gamma \subset \rho(\mathcal{K})$  be a closed Jordan curve enclosing  $\lambda$  such that  $\sigma(\mathcal{K}) \cap \Delta = \{\lambda\}$ , where  $\Delta$  is the region inside  $\Gamma$ . Suppose Assumption 4.2 holds for all  $z \in \Gamma$ . Then we have

$$\lim_{N \rightarrow \infty} [\sigma(\mathcal{K}_N) \cap \Delta] = \{\lambda\}$$

in the Kuratowski sense [4, Chapter 5.1.1] (hence, implying Hausdorff convergence). Moreover, if Assumption 4.5 holds, we have  $\sigma(\mathcal{K}_N) \cap \Delta$  consists of exactly  $m$  eigenvalues, for  $N$  large enough.

*Proof of Theorem 4.10.* We show lower semicontinuity and upper semicontinuity (Remark 4.11), then prove multiplicity preservation.

*Lower semicontinuity.* Choose  $\varepsilon > 0$  small enough so that the circle

$$\gamma_\varepsilon := \{z : |z - \lambda| = \varepsilon\}$$

lies in  $\rho(\mathcal{K})$  and encloses no spectral point of  $\mathcal{K}$  other than  $\lambda$ . Let  $\mathcal{P}^{\gamma_\varepsilon}$  and  $\mathcal{P}_N^{\gamma_\varepsilon}$  be the Riesz projections defined by  $\gamma_\varepsilon$  (as in Definition 4.4). Then  $\dim(\mathcal{P}^{\gamma_\varepsilon} \mathcal{F}) = m$ . By Corollary 4.9 applied to the contour  $\gamma_\varepsilon$ , for  $N$  sufficiently large we have

$$\dim(\mathcal{P}_N^{\gamma_\varepsilon} \mathcal{F}) \geq m,$$

hence  $\mathcal{P}_N^{\gamma_\varepsilon} \neq 0$  and therefore  $\sigma(\mathcal{K}_N) \cap B(\lambda, \varepsilon) \neq \emptyset$ . In particular, there exists  $\lambda_N \in \sigma(\mathcal{K}_N) \cap \Delta$  such that  $|\lambda_N - \lambda| < \varepsilon$  for all large  $N$ .

*Upper semicontinuity.* Let  $\bar{\Delta}$  be the closure of  $\Delta$  and define the compact set

$$\bar{\Delta}_\varepsilon := \bar{\Delta} \setminus B(\lambda, \varepsilon).$$

Since  $\sigma(\mathcal{K}) \cap \bar{\Delta}_\varepsilon = \emptyset$ , we have  $\bar{\Delta}_\varepsilon \subset \rho(\mathcal{K})$ . Applying Lemma 4.6 to  $U = \bar{\Delta}_\varepsilon$  yields  $N(\varepsilon)$  such that for all  $N > N(\varepsilon)$ ,

$$\bar{\Delta}_\varepsilon \subset \rho(\mathcal{K}_N),$$

and hence  $\sigma(\mathcal{K}_N) \cap \bar{\Delta}_\varepsilon = \emptyset$ . Therefore every  $\mu \in \sigma(\mathcal{K}_N) \cap \Delta$  must satisfy  $|\mu - \lambda| < \varepsilon$ . Since  $\varepsilon > 0$  is arbitrary, every limit point of  $\sigma(\mathcal{K}_N) \cap \Delta$  equals  $\lambda$ .

*Multiplicity preservation.* Assume Assumption 4.5 holds, so  $\dim(\mathcal{P}_N^\lambda \mathcal{F}) = m$  for  $N$  large enough. Then the finite-dimensional operator  $\mathcal{P}_N^\lambda \mathcal{K}_N \mathcal{P}_N^\lambda$  acting on  $\mathcal{P}_N^\lambda \mathcal{F}$  has dimension  $m$ , and its spectrum equals  $\sigma(\mathcal{K}_N) \cap \Delta$  (Riesz decomposition, cf. [4, Theorem 2.27]). Hence  $\sigma(\mathcal{K}_N) \cap \Delta$  consists of exactly  $m$  eigenvalues, counting algebraic multiplicities.  $\square$

**Remark 4.11.** Intuitively speaking, upper semicontinuity ensures that every limit of approximate spectral points is contained in the true spectrum, which prevents irrelevant points (i.e., *spectral pollution*) and lower semicontinuity ensures that every point of the true spectrum is approached by some approximate spectral points, which prevents loss of spectral points (i.e., *spectral inclusion*).

**Remark 4.12.** The [4, Theorem 2.27] in the above theorem mainly says that one can construct a spectral projection via a contour integral, which decomposes the space into two invariant subspaces: one that contains exactly the isolated part of the spectrum and one that contains the remainder. Essentially, it provides a method to “split” or reduce  $\mathcal{K}$  into simpler parts corresponding to these separated spectral regions.

**Remark 4.13.** In a compact metric space (or for compact sets), Kuratowski convergence implies Hausdorff convergence because the topological constraints (via lower and upper limits) force the sets to become metrically close in the Hausdorff distance.

Now we want to extend the Hausdorff convergence result beyond isolated eigenvalues to a compact subset of the spectrum. In order to do so, we need to introduce a new concept called *resolvent stability* as follows.

**Definition 4.14** (Resolvent Stability). Let  $\{\mathcal{K}_N\}$  be a sequence of closed linear operators on a Banach space  $\mathcal{F}$ , and let  $U$  be a compact subset of  $\mathbb{C}$ . The sequence  $\{\mathcal{K}_N\}$  is said to be *resolvent stable around  $U$*  if there exists a neighborhood  $N(U)$  of  $U$  such that for any  $z \in N(U) \setminus U$ , we have

$$\liminf_{N \rightarrow \infty} \text{dist}(\sigma(\mathcal{K}_N), z) > 0 \Rightarrow \limsup_{N \rightarrow \infty} \|\mathcal{R}(z, \mathcal{K}_N)\| < \infty.$$

**Remark 4.15.** Equivalently speaking, we can also say that  $N(U) \setminus U$  has the  $\{\mathcal{K}_N\}$ -Resolvent Condition, where the  $\{\mathcal{K}_N\}$ -Resolvent Condition for a point  $z \in \mathbb{C}$  means that

$$\liminf_{N \rightarrow \infty} \text{dist}(\sigma(\mathcal{K}_N), z) > 0 \Rightarrow \limsup_{N \rightarrow \infty} \|\mathcal{R}(z, \mathcal{K}_N)\| < \infty.$$

The *resolvent stability* property prevents the formation of spurious eigenvalues in the vicinity of the compact subset  $U$ , which is necessary for proving the lower semicontinuity in the spectral convergence.

**Theorem 4.16.** Let  $\mathcal{K}$  be a bounded Koopman operator and  $\{\mathcal{K}_N\}_{N \in \mathbb{N}}$  be finite-dimensional approximations that converge strongly to  $\mathcal{K}$  and satisfy Assumption 4.2. Let  $U \subset \sigma(\mathcal{K})$  be a non-empty compact subset enclosed by a positively oriented contour  $\Gamma \subset \rho(\mathcal{K})$ , and let  $\Delta$  denote the interior of  $\Gamma$ . Assume  $\sigma(\mathcal{K}) \cap \Delta = U$  (equivalently,  $\Delta \setminus U \subset \rho(\mathcal{K})$ ). Then

$$\liminf_{N \rightarrow \infty} \text{dist}(U, \sigma(\mathcal{K}_N) \cap \Delta) = 0,$$

i.e. the spectrum of  $\mathcal{K}_N$  is lower semicontinuous at  $U$ .

*Proof.* Because  $\Delta \setminus U \subset \rho(\mathcal{K})$  by assumption, every  $z \in \Delta \setminus U$  lies in the resolvent set of  $\mathcal{K}$ . Assumption 4.2 therefore yields constants  $N_z \in \mathbb{N}$  and  $M_z > 0$  such that for all  $N > N_z$ ,

$$z \in \rho(\mathcal{K}_N) \quad \text{and} \quad \|\mathcal{R}_N(z)\| \leq M_z,$$

where  $\mathcal{R}_N(z) = (zI - \mathcal{K}_N)^{-1}$ .

Fix  $z \in \Delta \setminus U$  and assume  $\liminf_{N \rightarrow \infty} \text{dist}(\sigma(\mathcal{K}_N), z) > 0$ . Then there exist  $\delta > 0$  and  $N_0$  such that  $\text{dist}(\sigma(\mathcal{K}_N), z) > \delta$  for all  $N > N_0$ . Consequently, for every  $N > \max\{N_0, N_z\}$  we have the uniform bound  $\|\mathcal{R}_N(z)\| \leq M_z$ . Hence the sequence  $\{\mathcal{K}_N\}$  is *resolvent-stable* around  $U$  in the sense of Definition 4.14 (take  $N(U) = \Delta$ ).

Applying Mills' theorem [25, Theorem 3.2], which requires strong convergence and resolvent stability around  $U$ , gives

$$\liminf_{N \rightarrow \infty} \text{dist}(U, \sigma(\mathcal{K}_N) \cap \Delta) = 0,$$

which is the desired lower semicontinuity.  $\square$

**Remark 4.17.** Upper semicontinuity in Theorem 4.16 is not satisfied unless we have a stronger condition that  $\mathcal{K}_N$  uniformly converges to  $\mathcal{K}$ . Refer to [14, Theorem 3.1, Chapter 4] for more details.

We want to point out that Chatelin's work in [4] primarily addresses the convergence of isolated eigenvalues which provides a comprehensive framework that ensures preservation of algebraic multiplicities during the approximation process. This is particularly valuable for numerical analysis as it guarantees that the number of approximate eigenvalues (counting multiplicity) matches that of the exact operator. In contrast, Mills' work in [25] extends spectral convergence theory (i.e., lower semicontinuity) to compact subsets of the spectrum, which offers a much broader applicability beyond just isolated eigenvalues.

## 5 Error Bounds Analysis

In the last section, we established the convergence of the approximated spectrum  $\sigma(\mathcal{K}_N)$  to the true spectrum  $\sigma(\mathcal{K})$ . However, for practical application, it is essential to quantify the error of a computed solution. In this section, we will derive an error bound for the computed eigenvalues that is controlled by a residual quantity  $\eta_N$ , as defined later. This provides a practical way to assess the accuracy of the spectral information obtained via Galerkin methods such as EDMD [34] and our pseudo-resolvent approach.

**Definition 5.1** (Arithmetic Mean of Approximate Eigenvalues). Let  $\lambda$  be an isolated eigenvalue of  $\mathcal{K}$  with algebraic multiplicity  $m_\lambda$ , and let  $\Gamma_\lambda$  be an isolating closed Jordan curve as defined in Definition 4.4. For  $N$  large enough, Assumption 4.5 guarantees that there are exactly  $m_\lambda$  eigenvalues of  $\mathcal{K}_N$  inside  $\Gamma_\lambda$ , which we denote by  $\{\mu_{N,j}\}$  for  $j = 1, \dots, m_\lambda$ , counting multiplicities. We define their arithmetic mean as:

$$\bar{\lambda}_N := \frac{1}{m_\lambda} \sum_{j=1}^{m_\lambda} \mu_{N,j}. \quad (9)$$

**Definition 5.2.** Let  $\mathcal{P}_N^\lambda$  be the spectral projection associated with the eigenvalues of  $\mathcal{K}_N$  inside the contour  $\Gamma_\lambda$ . We define the residual quantity  $\eta_N$  as:

$$\eta_N := \|(\mathcal{K} - \mathcal{K}_N)\mathcal{P}_N^\lambda\|.$$

To support our main proof, we state a key lemma from spectral approximation theory in the following, which establishes the fundamental relationship between the error in the mean eigenvalue and the trace of an operator difference.

**Lemma 5.3.** Let  $\lambda$  be an isolated eigenvalue of  $\mathcal{K}$  with finite algebraic multiplicity  $m$ , and  $\mathcal{M}$  be the associated invariant subspace. Consider the operator  $\mathcal{G}_N := \mathcal{K}_N|_{\mathcal{M}}$ , which is the restriction of the Galerkin approximation  $\mathcal{K}_N$  to

the true invariant subspace  $\mathcal{M}$ . Let  $\bar{\lambda}$  be the arithmetic mean of the  $m$  eigenvalues of the finite-dimensional operator  $\mathcal{G}_N$ . Denoting these eigenvalues by  $\{\mu_{N,j}\}_{j=1}^m$ , the arithmetic mean is defined as:

$$\bar{\lambda} := \frac{1}{m} \sum_{j=1}^m \mu_{N,j}.$$

Then, we have the following identity:

$$\lambda - \bar{\lambda} = \frac{1}{m} \text{tr}((\mathcal{K} - \mathcal{K}_N)|_{\mathcal{M}}).$$

**Theorem 5.4.** Let  $\lambda$  be an isolated eigenvalue of the Koopman operator  $\mathcal{K}$  with finite algebraic multiplicity  $m_\lambda$ . Let  $\Gamma_\lambda$  be a closed Jordan curve isolating  $\lambda$  from the rest of  $\sigma(\mathcal{K})$ . Suppose that Assumption 4.2 and Assumption 4.5 hold. Then for  $N$  sufficiently large, the error in the arithmetic mean of the approximate eigenvalues is bounded by the residual  $\eta_N$  in Definition 5.2. Specifically, there exists a constant  $C$  independent of  $N$  such that

$$|\lambda - \bar{\lambda}_N| \leq C \cdot \eta_N. \quad (10)$$

*Proof.* Let  $\mathcal{M}_N^\lambda := \mathcal{P}_N^\lambda \mathcal{F}$ , which has dimension  $m_\lambda$  for all large  $N$  by Assumption 4.5. The eigenvalues of  $\mathcal{K}_N$  inside  $\Gamma_\lambda$  (counting algebraic multiplicity) are exactly the eigenvalues of the finite-dimensional operator  $\mathcal{G}_N := \mathcal{K}_N|_{\mathcal{M}_N^\lambda}$ , hence

$$\bar{\lambda}_N = \frac{1}{m_\lambda} \text{tr}(\mathcal{G}_N).$$

The desired a posteriori estimate is a direct consequence of [4, Theorem 6.15], which gives a constant  $C$  independent of  $N$  under stable and strongly stable convergence such that

$$|\lambda - \bar{\lambda}_N| \leq C \|(\mathcal{K} - \mathcal{K}_N)\mathcal{P}_N^\lambda\|.$$

By Definition 5.2, the right-hand side equals  $C\eta_N$ . This completes the proof.  $\square$

**Remark 5.5.** A numerical verification for this error bound is presented in Section 6.2.

## 6 Experiments

### 6.1 Pendulum

In this experiment, data is generated by simulating a single undamped pendulum. From a physics perspective, this system is a conservative Hamiltonian system. Its trajectories preserve total energy, and the dynamics are characterized by the oscillations. Consequently, the true spectrum of the Koopman operator is expected to lie strictly on the unit circle, while the corresponding generator spectrum should lie on the imaginary axis.

The simulation involves a single trajectory of 1500 time steps with a fixed sampling interval of 0.2 seconds. The system is initialized from a random state, where the angle  $\theta$  is drawn uniformly from 0 to  $2\pi$  and the angular velocity  $\dot{\theta}$  from  $-5$  to  $5$ . The underlying dynamics are governed by the nonlinear equation:

$$\ddot{\theta} = -\frac{3g}{2l} \sin(\theta),$$

with gravitational acceleration  $g = 9.8$  and pendulum length  $l = 1.0$ . The angular acceleration is computed at each step, and the state is updated via Euler's method. For the dictionary, we employ a hybrid basis: a Fourier basis for the periodic angle  $\theta$  (using  $\exp\{in\theta\}$  for  $n \in [-20, 20]$ ) and a Hermite polynomial basis for the unbounded angular velocity  $\dot{\theta}$  (up to order 30, with velocity rescaled by  $1/\sqrt{2}$ ). These basis functions are multiplied to form the dictionary of observables used to approximate the resolvent and analyze the spectral properties.

Figure 1 illustrates the behavior of the inverse resolvent norm,  $1/\|\mathbf{R}(z, \mathbf{K}_N)\|$ , as the probe  $z$  traverses circles with radii  $\Gamma_{1.01}$ ,  $\Gamma_{1.25}$ , and  $\Gamma_{1.5}$ . Theoretically, as  $z$  approaches the true spectrum (the unit circle), the resolvent norm should diverge, causing its inverse to vanish. This behavior is clearly observed: the value of  $1/\|\mathbf{R}(z, \mathbf{K}_N)\|$  decreases significantly as the radius approaches 1. Consequently, by refining the detection threshold, only grid points in close proximity to the unit circle are identified as spectral candidates, thereby enhancing the precision of the approximation.

In Figure 2, we compare the Koopman operator  $\mathbf{K}_N$  approximated via standard EDMD against the resolvent operator  $\mathbf{R}(z, \mathbf{K}_N)$  computed using our method. We utilize dictionary sizes of 225, 361, 600, and 702 functions on a separate simulated dataset, testing thresholds of  $2.5 \times 10^{-14}$  and  $3.5 \times 10^{-14}$ . The probe points  $z$  are distributed along  $\Gamma_{1.01}$ , a

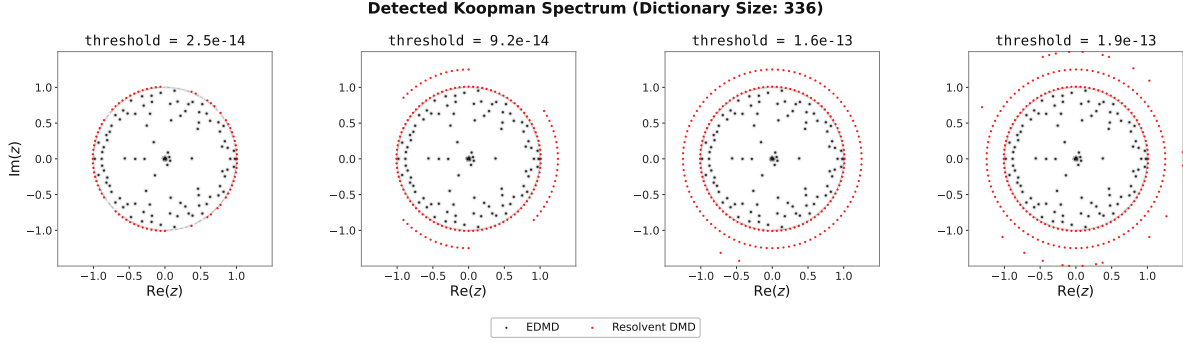


Figure 1: Koopman spectrum of the nonlinear pendulum: EDMD eigenvalues (black) and resolvent-based detection (red) under successive threshold refinement.

slight perturbation of the unit circle chosen to avoid numerical singularities. As the dictionary size  $N$  increases, the indicator  $1/\|\mathbf{R}(z, \mathbf{K}_N)\|$  diminishes for a larger proportion of grid points. This leads to a higher detection rate along  $\Gamma_{1.01}$  for a fixed threshold, which suggests a clear convergence behavior as the approximation subspace grows.

In Figure 3, we further evaluate the continuous-time Koopman generator using the pseudo-resolvent matrix from Eq. (6). Consistent with the conservative nature of the system described at the outset, we verify whether the detected spectrum aligns with the imaginary axis. To avoid singularities, we sample the resolvent indicator on two vertical lines  $\Re(z) = \pm 0.01$  flanking the imaginary axis. Using the criterion  $1/\|\mathbf{R}(z, \mathbf{A}_N)\| < \varepsilon$ , we observe that as  $\varepsilon$  is relaxed from  $10^{-14}$  to  $10^{-12}$ , the detected set expands but remains tightly concentrated near the imaginary axis. This accurately reflects the physically expected purely oscillatory behavior without introducing artificial damping.

For comparison, Figure 4 displays the generator spectrum obtained via gEDMD [17]. In the gEDMD approach (or equivalently, mapping discrete EDMD eigenvalues  $\mu_j$  via the principal logarithm  $\lambda_j \approx \Delta t^{-1} \log \mu_j$ ), the spectrum exhibits a significant spread into the left half-plane. This phenomenon indicates *spurious dissipation*: the finite-dimensional truncation causes the eigenvalues to contract inside the unit circle ( $|\mu_j| < 1$ ), which the logarithm translates into negative real parts ( $\Re(\lambda_j) < 0$ ). This artificial decay violates the conservation of energy inherent to the pendulum. In contrast, our pseudo-resolvent approach avoids the direct matrix logarithm and successfully preserves the Hamiltonian spectral structure along the imaginary axis.

Finally, Figure 5 presents a sensitivity analysis regarding the detection threshold  $\varepsilon$  over the range  $[10^{-16}, 10^{-10}]$ . The curve tracks the number of detected spectral points out of a total of 60 test probes located along two vertical lines  $\Re(z) = \pm 0.01$ , designed to probe the generator spectrum along the imaginary axis. We observe a sharp phase transition in the detection count: below the threshold  $10^{-14}$ , no points are detected; however, as  $\varepsilon$  increases, the count rises rapidly until reaching a saturation status where all 60 points are successfully identified (e.g.,  $0/60 \rightarrow 39/60 \rightarrow 60/60$ ). This saturation indicates that the physical spectrum is well-separated from the underlying numerical errors without the need for precise threshold tuning. Collectively, these results demonstrate that the computed singular values exhibit a clear separation between spectral and non-spectral regions, which confirms that the resolvent norm criterion provides a robust diagnostic for identifying the generator spectrum directly from data.

## 6.2 Linear oscillator

Consider the two-dimensional linear oscillator

$$\dot{x} = Ax \quad \text{with} \quad A = \begin{pmatrix} -0.3 & -2 \\ 2 & -0.3 \end{pmatrix},$$

discretized at  $\Delta t = 0.2$ . The Koopman eigenvalues of this system are analytically known:  $\lambda_{n_1, n_2} = z_1^{n_1} z_2^{n_2}$ , where  $z_{1,2} = e^{(-0.3 \pm 2i) \cdot 0.2}$  and  $|z_1| \approx 0.9418$ . We approximate the Koopman operator via EDMD with a Random Fourier Feature (RFF) [28] dictionary of size  $N \in \{20, 30, 50, 80, 120, 180, 250, 350, 500\}$  with kernel length-scale  $\ell = 1.5$ , giving the finite-section operator  $\mathcal{K}_N = \Psi_X^\dagger \Psi_Y \in \mathbb{R}^{N \times N}$ .

Theorem 5.4 asserts that, for each isolated eigenvalue  $\lambda$  of the Koopman operator  $\mathcal{K}$  with finite algebraic multiplicity  $m_\lambda$  (i.e.,  $|\lambda - \bar{\lambda}_N| \leq C \eta_N$ ), where  $\bar{\lambda}_N = m_\lambda^{-1} \sum_{j=1}^{m_\lambda} \mu_{N,j}$  is the arithmetic mean of the EDMD eigenvalues clustering around  $\lambda$  (for a simple eigenvalue, simply  $\mu_N$ ),  $C$  is a constant *independent of*  $N$ , and  $\eta_N$  is the operator-level truncation error defined in Definition 5.2 (i.e.,  $\eta_N = \|(\mathcal{K} - \mathcal{K}_N) \mathcal{P}_N^\lambda\|$ ) with  $\mathcal{P}_N^\lambda$  the spectral projection of  $\mathcal{K}_N$  associated with the eigenvalues near  $\lambda$ .

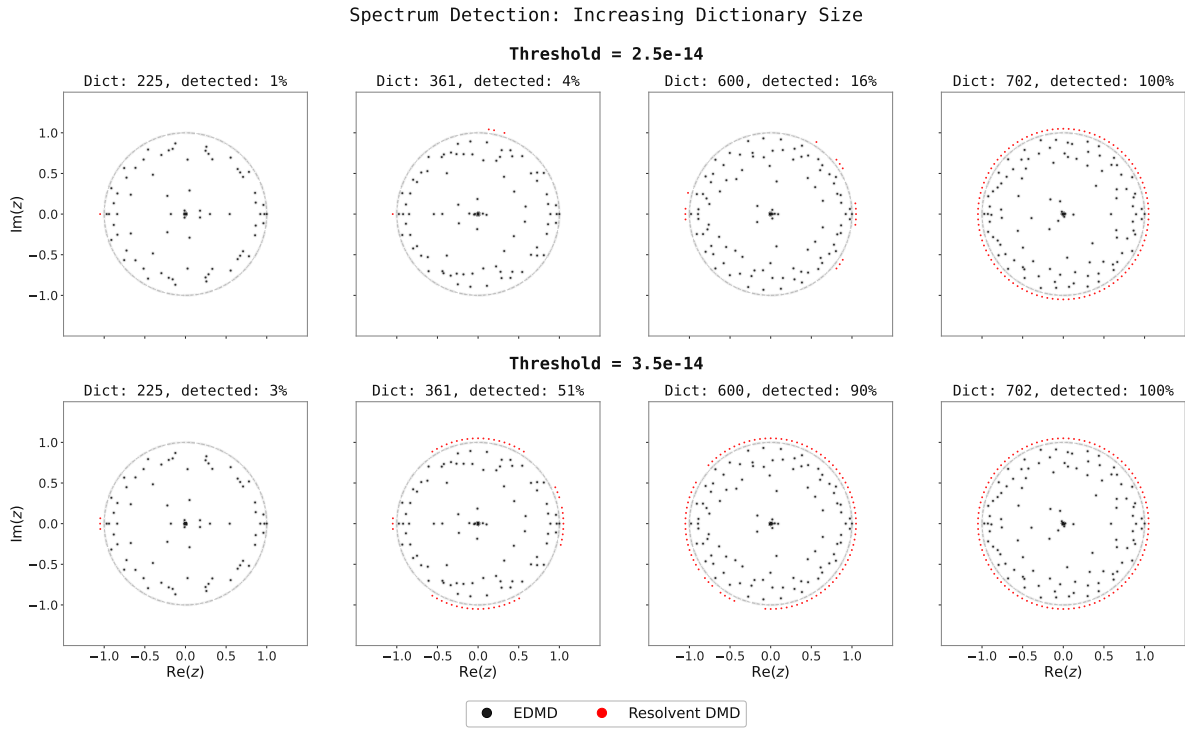


Figure 2: Effect of dictionary size on resolvent-based Koopman spectrum detection for the nonlinear pendulum: larger dictionary size gives higher detection rates under two different singular-value thresholds.

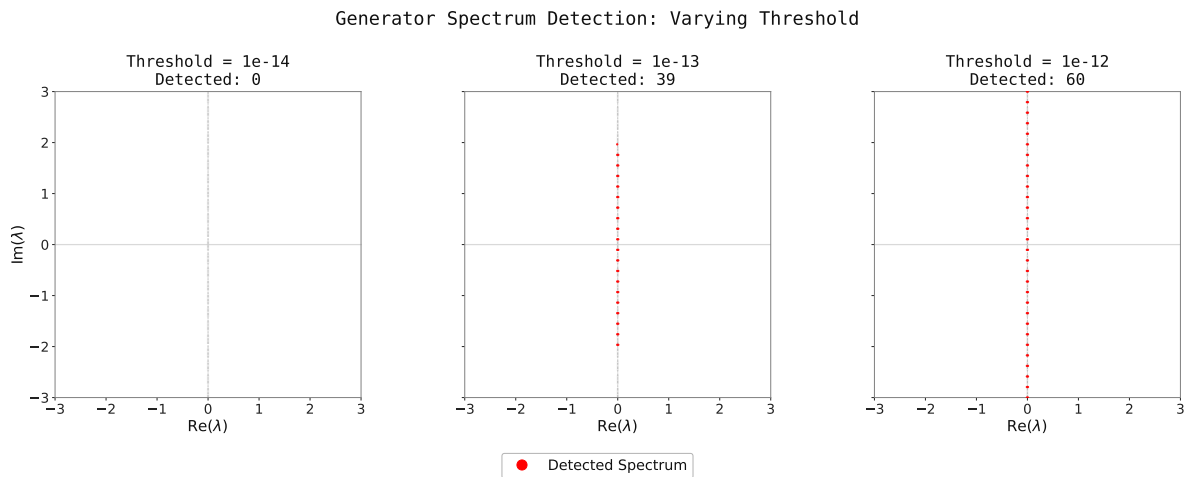


Figure 3: Resolvent-based detection of the Koopman generator spectrum along the imaginary axis under successive threshold refinement ( $\epsilon = 10^{-14}, 10^{-13}, 10^{-12}$ ).

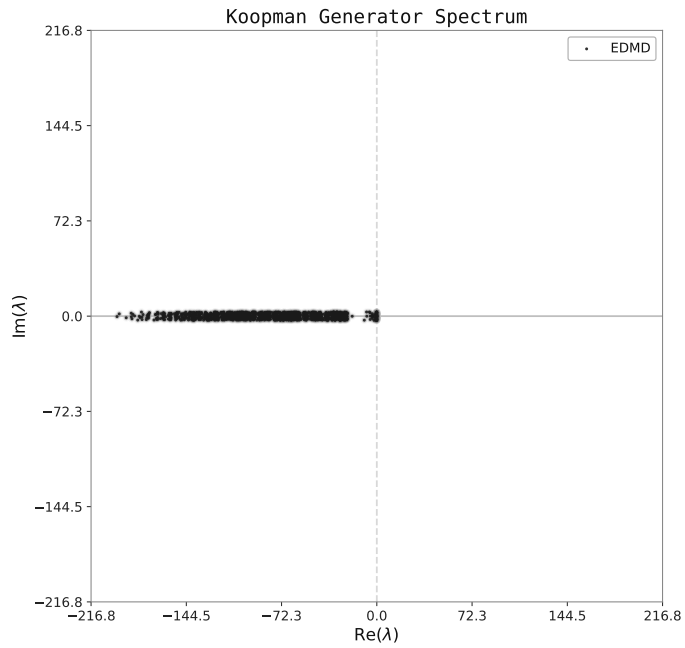


Figure 4: Spectrum of the EDMD-approximated Koopman generator for the nonlinear pendulum by taking the matrix logarithm of the Koopman operator.

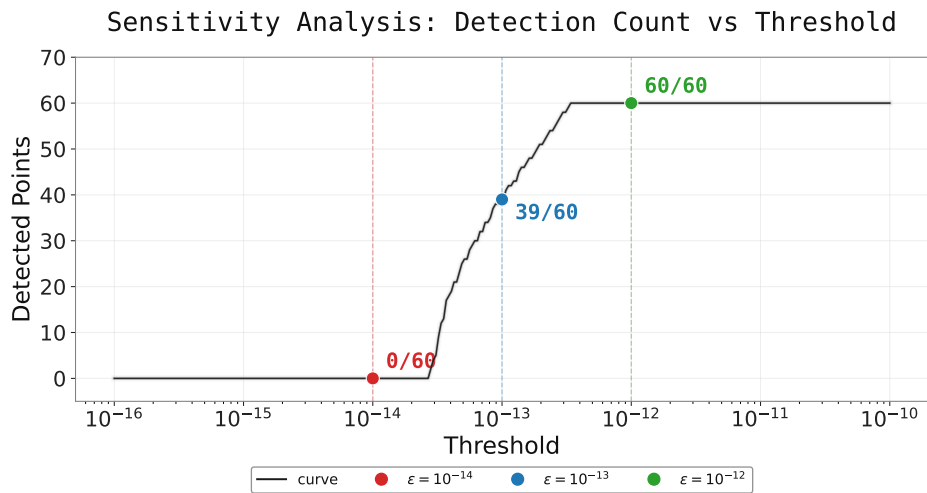


Figure 5: Sensitivity of spectrum detection to the varying singular-value threshold  $\epsilon$ : a sharp transition from 0 to full detection.

By definition, the Koopman operator acts as  $\mathcal{K}f(x) = f(T(x))$  for any observable  $f$ , where  $T$  is the discrete-time flow map. For a general nonlinear system,  $T$  is typically unknown and only accessible through data, making direct evaluation of  $(\mathcal{K} - \mathcal{K}_N)$  infeasible. Since the flow map  $T(x) = Mx$ ,  $M = e^{A\Delta t}$  of the linear oscillator is known in closed form, we can evaluate  $\mathcal{K}f(x) = f(Mx)$  at any point  $x$  for any observable  $f$ . This makes it possible to compute the truncation error  $(\mathcal{K} - \mathcal{K}_N)$  on any dictionary function directly, with no approximation beyond Monte Carlo quadrature.

For each target eigenvalue  $\lambda$  (all five are simple,  $m_\lambda = 1$ ), let  $v_N$  and  $w_N$  denote, respectively, the right and left eigenvectors of the EDMD matrix  $K_N$ , normalized so that  $w_N^H v_N = 1$ . The approximate eigenfunction is  $g_N(x) = \sum_j (v_N)_j \psi_j(x)$ , and the truncation error acts as

$$(\mathcal{K} - \mathcal{K}_N)g_N(x) = g_N(Mx) - \mu_N g_N(x),$$

since  $\mathcal{K}_N g_N = \mu_N g_N$  by construction, whereas  $\mathcal{K}g_N(x) = g_N(Mx) \neq \mu_N g_N(x)$  (the dictionary functions are not Koopman eigenfunctions). For a rank-one spectral projection  $\mathcal{P}_N^\lambda$ , the operator norm evaluates to

$$\eta_N = \sqrt{w_N^H G^{-1} w_N} \cdot \|(\mathcal{K} - \mathcal{K}_N)g_N\|_{L^2(\mu)}, \quad (11)$$

where  $G$  is the Gram matrix of the dictionary in  $L^2(\mu)$ . We estimate both the  $L^2$  norm and  $G$  via Monte Carlo integration with  $10^5$  i.i.d. samples drawn from the same distribution as the training data. Here  $G^{-1}$  is computed via a (regularized) pseudoinverse or Tikhonov regularization when needed.

Since  $C$  in Eq.(10) is unknown but  $N$ -independent, the theorem predicts that the ratio  $|\mu_N - \lambda|/\eta_N$  should remain bounded as  $N \rightarrow \infty$ . We therefore track this ratio across all dictionary sizes and modes as the verification strategy. For each dictionary size  $N$  and each of the five target modes  $\{(1, 0), (0, 1), (2, 0), (0, 2), (1, 1)\}$ , we identify the EDMD eigenvalue  $\mu_N$  closest to the true eigenvalue  $\lambda$  and compute  $\eta_N$  via Eq.(11).

Figure 6 plots the eigenvalue error  $|\mu_N - \lambda|$  against  $\eta_N$  on a log-log scale. All 45 data points (9 dictionary sizes  $\times$  5 modes) lie strictly below the diagonal  $|\mu_N - \lambda| = \eta_N$ , and also below the fitted line  $|\mu_N - \lambda| = C \eta_N$  with  $C = 0.04$ . Both  $|\mu_N - \lambda|$  and  $\eta_N$  decrease as  $N$  grows (visible from the annotations for mode  $(1, 0)$ ), and the two quantities decrease in a correlated fashion, as the theorem predicts.

Figure 7 provides a complementary view. The left panel shows the convergence of both  $|\mu_N - \lambda|$  (solid) and  $\eta_N$  (dashed) as functions of  $N$  for each mode; more specifically, the error is consistently several orders of magnitude smaller than  $\eta_N$ , and both decline with increasing  $N$ . The right panel plots the ratio  $|\mu_N - \lambda|/\eta_N$  versus  $N$ . Across all modes and dictionary sizes, the ratio remains bounded above by  $C_{\max} \approx 0.04$ , with no upward trend as  $N$  increases. The maximum observed ratio is

$$\max_{N, \lambda} \frac{|\mu_N - \lambda|}{\eta_N} = 0.042 \ll 1,$$

which confirms the existence of a finite,  $N$ -independent constant  $C$  as asserted by Theorem 5.4.

The fact that  $C_{\max} \ll 1$  indicates that the bound is conservative; more specifically, the eigenvalue error is roughly 25 times smaller than the truncation error  $\eta_N$ . This is indeed expected, because the theorem provides a worst-case guarantee over all directions in the spectral subspace, while the actual perturbation  $(\mathcal{K} - \mathcal{K}_N)$  projects only weakly onto the most sensitive direction of the resolvent.

### 6.3 Comparison of pseudospectral contours

In this subsection, we compare the spectral approximation capabilities of ResDMD and the proposed Resolvent DMD by examining their pseudospectral contours. The primary objective is to demonstrate the robustness of each method against spectral pollution and their ability to localize spectral components in the complex plane, particularly in regions away from the origin.

We consider the Lorenz 63 system, governed by the following differential equations:

$$\begin{aligned} \dot{x} &= \sigma(y - x), \\ \dot{y} &= x(\rho - sz) - y, \\ \dot{z} &= sxy - \beta z, \end{aligned} \quad (12)$$

where the system parameters are set to  $\sigma = 10.0$ ,  $\beta = 8/3$ , and  $\rho = 40.0$ , corresponding to a chaotic regime. A scaling factor  $s = 0.1$  is introduced to the nonlinear coupling terms to adjust the dynamic range of the state variables. Time-series data are generated by integrating a single trajectory with a time step of  $\Delta t = 0.05$ .

For the construction of the Koopman operator approximation, we employ a dictionary consisting of tensor products of normalized Hermite polynomials. To efficiently manage the dimensionality while capturing the essential dynamics,

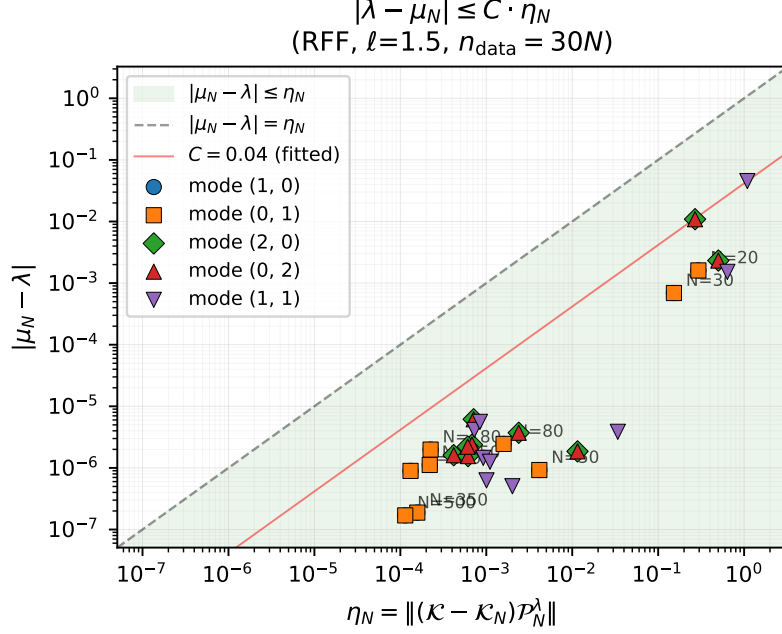


Figure 6: Eigenvalue error  $|\mu_N - \lambda|$  versus truncation error  $\eta_N = \|(\mathcal{K} - \mathcal{K}_N)\mathcal{P}_N^\lambda\|$  for five Koopman modes across nine dictionary sizes. The dashed diagonal marks  $|\mu_N - \lambda| = \eta_N$ ; the red line shows the fitted bound with  $C = 0.04$ . All points lie well below the diagonal, which confirms Eq. (10).

### Convergence and ratio boundedness

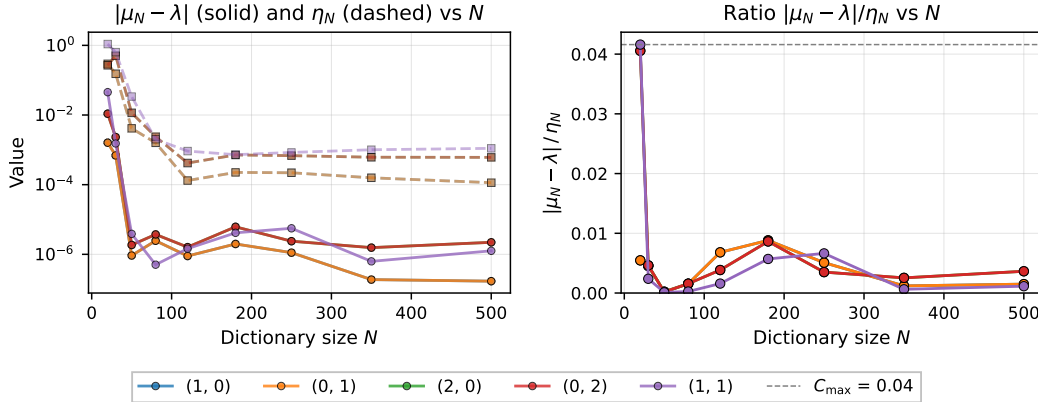


Figure 7: Left: convergence of  $|\mu_N - \lambda|$  (solid) and  $\eta_N$  (dashed) as  $N$  increases. Right: ratio  $|\mu_N - \lambda|/\eta_N$  versus  $N$ ; the dashed grey line marks the overall maximum  $C_{\text{max}} = 0.04$ . The ratio remains bounded, consistent with Theorem 5.4.

the basis functions are selected via a hyperbolic-cross truncation of the multi-index set. This procedure results in a dictionary size of  $N = 110$ . Inner products are approximated using Gauss–Hermite quadrature.

We analyze the pseudospectra contours for both methods, which are computed as the level sets of the inverse of the resolvent norm,  $1/\|\mathbf{R}_N(z)\|$ . This quantity serves as a reliable indicator of the approximate spectrum; regions with large resolvent norms (i.e., small inverse values) correspond to the location of spectral points.

Figure 8 presents the comparison of pseudospectral contours computed using ResDMD (left) and Resolvent DMD (right). In the ResDMD result, the contours exhibit irregular distortions and isolated "islands" in the complex plane, indicating the presence of spurious eigenvalues and spectral pollution. In contrast, the Resolvent DMD result displays smooth contours that are sharply localized along the real axis. This indicates that Resolvent DMD more accurately

recovers the spectral components of the continuous-time generator, which typically lie along the real axis for dissipative chaotic attractors, and effectively suppresses the spectral pollution observed in ResDMD.

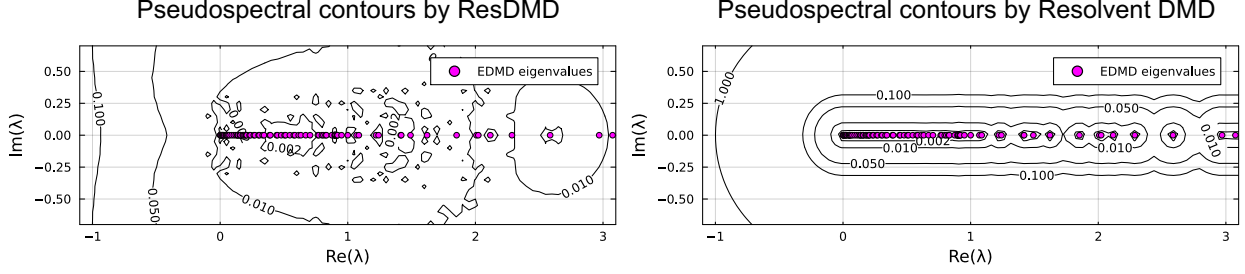


Figure 8: Pseudospectral contours computed by ResDMD (left) and Resolvent DMD (right) for the Lorenz system. The contours represent the level sets of the inverse resolvent norm,  $1/\|\mathbf{R}_N(z)\|$ . The pink dots indicate the eigenvalues computed by standard EDMD. Resolvent DMD demonstrates sharper localization along the real axis with significantly reduced spectral pollution compared to the distortions observed in ResDMD.

#### 6.4 Clustering two oscillators with thermal noise

We next compare Resolvent DMD with ResDMD on a pair of weakly damped oscillators observed under thermal and measurement noise. Both methods are designed to suppress spectral pollution, but this example probes their ability to separate two physical modes whose spectral supports are close and therefore difficult to distinguish.

We consider two second-order oscillators with viscous damping and additive thermal noise,

$$\ddot{x}_1(t) = -2\zeta\omega_1\dot{x}_1(t) - \omega_1^2x_1(t) + \sigma_1\eta_1(t), \quad (13)$$

$$\ddot{x}_2(t) = -2\zeta\omega_2\dot{x}_2(t) - \omega_2^2x_2(t) + \sigma_2\eta_2(t), \quad (14)$$

with  $\omega_1 = 3\pi/5$ ,  $\omega_2 = 3 \cdot 2\pi/5$ , damping ratio  $\zeta = 0.2$ , and noise intensities  $\sigma_1 = 0.05$ ,  $\sigma_2 = 0.15$ . The observed scalar signal is

$$x(t) = x_1(t) + x_2(t) + \xi(t), \quad (15)$$

where  $\xi(t)$  is zero-mean Gaussian measurement noise with standard deviation 0.015. We integrate the stochastic system on  $[0, 190]$  with time step  $\Delta t = 0.1$  and subsample to obtain  $M = 1050$  snapshots. From this single noisy trajectory we construct time-delay embedded data matrices  $\Psi_X, \Psi_Y$  of width  $N = 850$ .

Using quadrature-weighted inner products, we form the Gram matrix  $G = \Psi_X^* W \Psi_X$  and the cross matrix  $A = \Psi_X^* W \Psi_Y$ , where  $W = \text{diag}(w_m)$  contains the snapshot weights. The entries  $G_{i,j} = \langle \psi_i, \psi_j \rangle$  and  $A_{i,j} = \langle \mathcal{K}\psi_i, \psi_j \rangle$  define a finite-dimensional Galerkin approximation of the Koopman operator, and we obtain a matrix approximation

$$\mathcal{K}_N = G^\dagger A \approx (\Psi_X^* W \Psi_X)^\dagger (\Psi_X^* W \Psi_Y). \quad (16)$$

Throughout this example we take  $w_m = 1/M$  for randomly sampled snapshots [16, 20].

In our setting, both ResDMD and the proposed Resolvent DMD are designed to evaluate, from data, the spectrum of the Koopman operator—including its continuous component—but they do so using different constructions. ResDMD constructs, for each point  $z$  in the complex plane, a residual which, up to known scaling factors, is essentially the reciprocal of the resolvent norm of the Koopman operator. Resolvent DMD instead works directly with the finite-dimensional resolvent approximation  $\mathbf{R}_N(z)$  defined in Eq. (4) and Eq. (5). For each  $z$ , we take the dominant eigendirection of this resolvent (the eigenvector associated with its largest amplification) and regard the corresponding dictionary-based observable as a pseudoeigenfunction. Thus, the two methods approximate the same underlying resolvent quantity via reciprocal summaries: ResDMD uses residuals, whereas Resolvent DMD acts directly on the resolvent and its dominant eigendirections. In the present two-oscillator experiment, this direct resolvent-based construction yields a more accurate finite-dimensional approximation and, as we show below, a clearer separation of nearby spectral components than the residual-based ResDMD surrogate.

To compare the dynamic features extracted by ResDMD and Resolvent DMD, we follow the clustering framework in [29]. For each method, we collect a family of pseudoeigenfunctions  $\{g(z)\}$  over a grid of  $z$  in the complex plane. We then compute kernel principal angles between the subspaces spanned by these pseudoeigenfunctions, construct a similarity matrix from these angles, and apply spectral clustering to obtain a low-dimensional feature representation.

Finally, we perform fuzzy C-means clustering in this embedded feature space to account for ambiguity induced by continuous spectra and obtain three clusters that we interpret as candidate dynamic components.

Figure 9 shows the clustering results in the embedded feature space for ResDMD (left) and Resolvent DMD (right). In the Resolvent DMD case, the three clusters occupy well-separated regions, with clear gaps between the groups associated with the two physical modes and the residual high-frequency/noise-like components. In contrast, for ResDMD the regions corresponding to Cluster 2 and Cluster 3 lie in a largely overlapping portion of the feature space, and their boundary is much less distinct. This indicates that, although both methods are based on the same resolvent of the Koopman operator, the pseudoeigenfunctions produced by Resolvent DMD are more cleanly partitioned into three coherent groups in the embedded space, while the ResDMD pseudoeigenfunctions exhibit stronger mixing between two of the clusters.

To connect the clustering in the embedded space with spectral information, we compute spectral measures from the pseudoeigenfunctions using the rigorous resolvent-based procedure developed in [5]. Figure 10 shows the resulting spectral measures colored by cluster labels for ResDMD (left) and Resolvent DMD (right). In the Resolvent DMD case, the two broad peaks associated with the physical oscillation frequencies are each assigned predominantly to a distinct cluster, and a third cluster captures the remaining higher-frequency components. Thus the cluster structure aligns well with the two physical spectral peaks. In the ResDMD case, however, the cluster assignment on the low-frequency side is substantially mixed: the spectral contribution around the lower physical peak is not cleanly separated from nearby components, and the resulting clusters no longer correspond clearly to the two physical modes. This suggests that, when two physical modes occupy nearby spectral regions, Resolvent DMD has higher discriminative power than ResDMD in separating those modes, even though both methods share the goal of mitigating spectral pollution.

Finally, Figure 11 examines the cluster assignments at the level of the original time series. For each method, we reconstruct mode contributions by projecting the signal onto the clustered pseudoeigenfunctions and summing the components within each cluster. In the ResDMD reconstruction (left), the mode associated with the low-frequency cluster does not reproduce the correct low-frequency behavior; leakage from other components is visible, consistent with the failure to isolate the lower spectral peak in Figure 10. By contrast, the Resolvent DMD reconstruction (right) yields two components that closely match the two physical modes in both frequency and temporal modulation. These reconstructions corroborate the spectral-measure analysis and indicate that, in this example with two nearby spectral bands, Resolvent DMD achieves a more reliable separation of physical modes than ResDMD, while still pursuing the shared objective of suppressing spectral pollution.

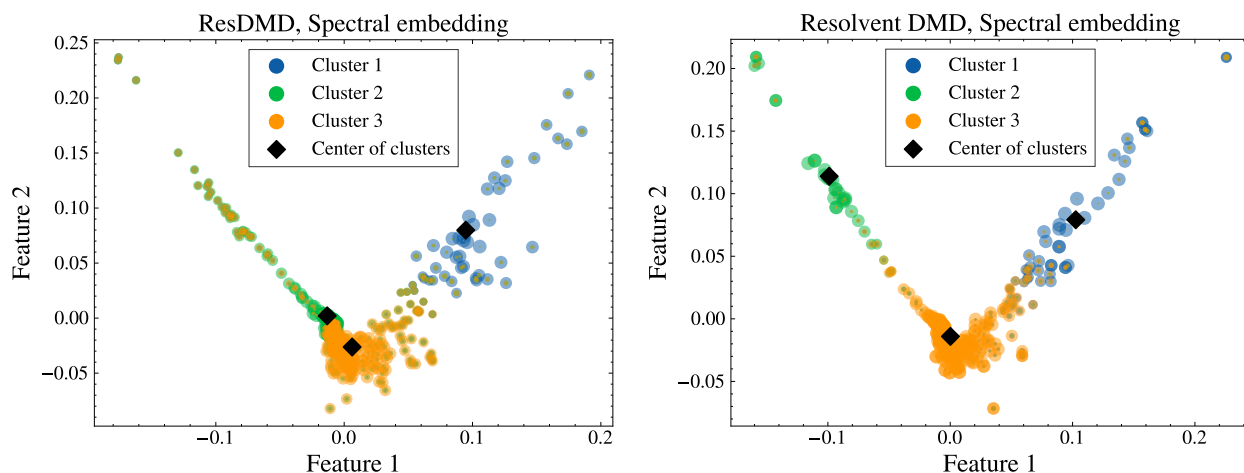


Figure 9: Clustering in the embedded feature space for ResDMD (left) and Resolvent DMD (right). Resolvent DMD produces three clearly separated clusters, whereas for ResDMD the regions corresponding to Cluster 2 and Cluster 3 lie close together with a blurred boundary.

## 7 Conclusion

In this work, we have presented a novel data-driven framework for the spectral analysis of the Koopman operator through the lens of pseudo-resolvents. By leveraging the Sherman-Morrison-Woodbury identity, we constructed a direct matrix approximation of the resolvent operator based on Galerkin approximations for spectral detection. Our theoretical

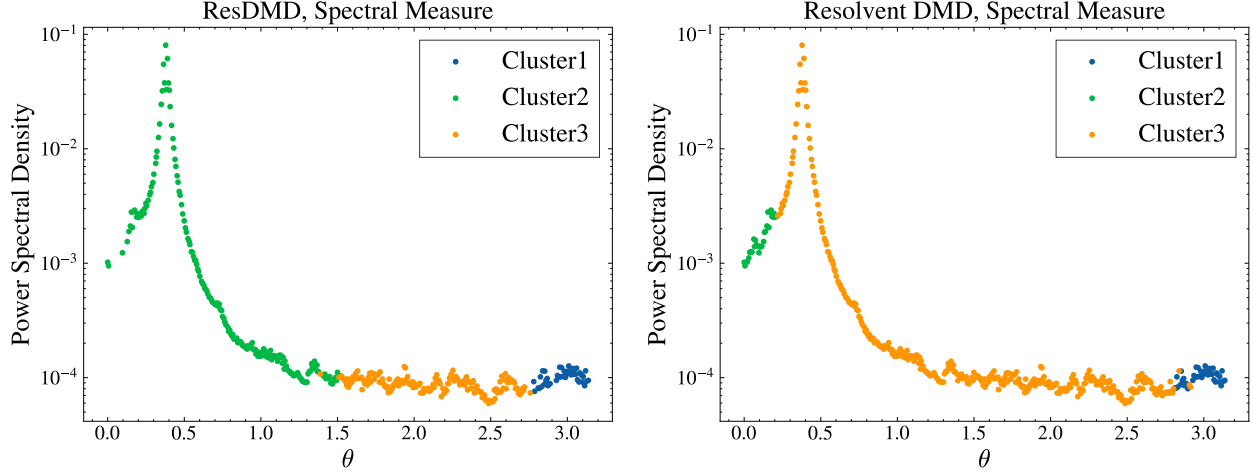


Figure 10: Clustering of spectral measures for ResDMD (left) and Resolvent DMD (right), computed using the resolvent-based procedure of [5]. Resolvent DMD separates the two physical peaks into distinct clusters, whereas ResDMD does not clearly isolate the lower-frequency peak.

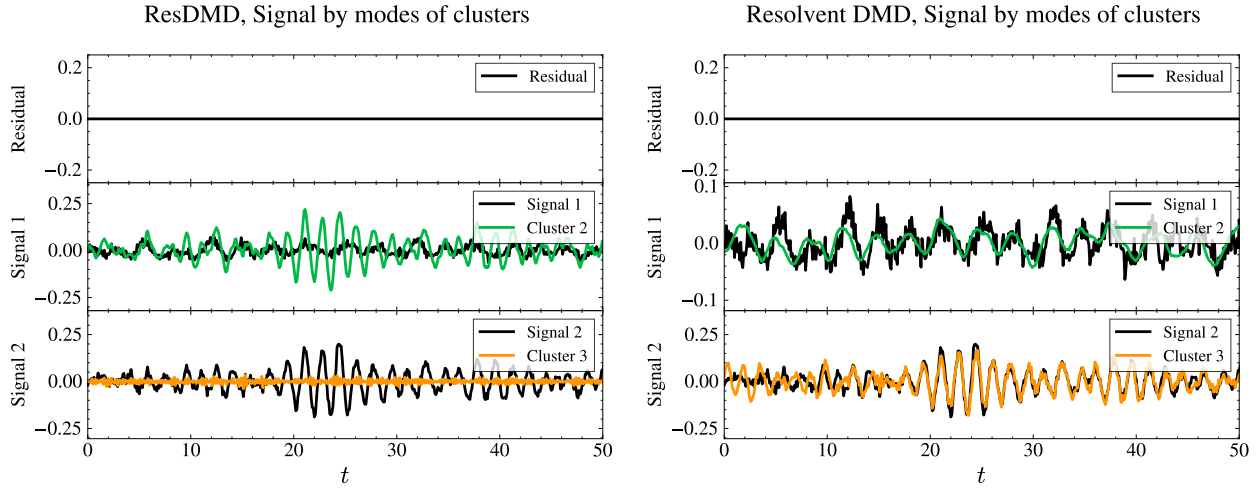


Figure 11: Reconstruction of the original signal from clustered pseudoeigenfunctions for ResDMD (left) and Resolvent DMD (right). Resolvent DMD recovers the two physical modes accurately, whereas the ResDMD-based reconstruction fails to reproduce the low-frequency component.

analysis establishes that the proposed method ensures spectral convergence in the Hausdorff metric under the resolvent stability conditions. Furthermore, we derived rigorous error bounds for the arithmetic mean of approximate eigenvalues, controlled by a residual quantity  $\eta_N$ . This offers a quantifiable measure of reliability that is often missing in most other heuristic DMD approaches.

Several directions remain open for future work, including local error bounds for eigenfunction approximations, extension of the theoretical framework to continuous-time generators using semigroup theory, and the development of principled guidelines for dictionary selection that ensure the stable convergence assumption is satisfied.

## Acknowledgment

Y.X. and I.I. acknowledge support from JST CREST Grant Number JPMJCR24Q1 including AIP challenge program, Japan. I.S. acknowledges support from JSPS KAKENHI Grant Number JP24K20864.

## References

- [1] DV Ansov. Geodesic flows on closed riemannian manifolds with negative curvature. In *Proc. Steklov Inst. Math.*, volume 90, pages 1–235, 1969.
- [2] George David Birkhoff. *Dynamical systems*, volume 9. American Mathematical Soc., 1927.
- [3] Marko Budišić, Ryan Mohr, and Igor Mezić. Applied koopmanism. *Chaos: An Interdisciplinary Journal of Nonlinear Science*, 22(4), 2012.
- [4] F. Chaitin-Chatelin. *Spectral Approximation of Linear Operators*. Computer science and applied mathematics. Academic Press, 1983.
- [5] Matthew J Colbrook and Alex Townsend. Rigorous data-driven computation of spectral properties of koopman operators for dynamical systems. *Communications on Pure and Applied Mathematics*, 77(1):221–283, 2024.
- [6] John B Conway. *A course in functional analysis*. Springer, 2019.
- [7] Weiyang Ding and Jie Li. Higher order extended dynamic mode decomposition based on the structured total least squares. *SIAM Journal on Scientific Computing*, 45(2):A985–A1011, 2023.
- [8] K.J. Engel, S. Brendle, R. Nagel, M. Campiti, T. Hahn, G. Metafuno, G. Nickel, D. Pallara, C. Perazzoli, A. Rhandi, et al. *One-Parameter Semigroups for Linear Evolution Equations*. Graduate Texts in Mathematics. Springer New York, 1999.
- [9] Dimitrios Giannakis and Claire Valva. Consistent spectral approximation of koopman operators using resolvent compactification. *Nonlinearity*, 37(7):075021, 2024.
- [10] Philip Hartman. A lemma in the theory of structural stability of differential equations. *Proceedings of the American Mathematical Society*, 11(4):610–620, 1960.
- [11] Philip Hartman. *Ordinary differential equations*. SIAM, 2002.
- [12] Benjamin Herrmann, Peter J Baddoo, Richard Semaan, Steven L Brunton, and Beverley J McKeon. Data-driven resolvent analysis. *Journal of Fluid Mechanics*, 918:A10, 2021.
- [13] Isao Ishikawa, Yuka Hashimoto, Masahiro Ikeda, and Yoshinobu Kawahara. Koopman operators with intrinsic observables in rigged reproducing kernel hilbert spaces. *Nonlinearity*, 38(11):115022, 2025.
- [14] T. Kato. *Perturbation Theory for Linear Operators*. Classics in Mathematics. Springer Berlin Heidelberg, 1995.
- [15] Anatole Katok, AB Katok, and Boris Hasselblatt. *Introduction to the modern theory of dynamical systems*. Number 54. Cambridge university press, 1995.
- [16] Stefan Klus, Péter Koltai, and Christof Schütte. On the numerical approximation of the perron-frobenius and koopman operator. *arXiv preprint arXiv:1512.05997*, 2015.
- [17] Stefan Klus, Feliks Nüske, Sebastian Peitz, Jan-Hendrik Niemann, Cecilia Clementi, and Christof Schütte. Data-driven approximation of the koopman generator: Model reduction, system identification, and control. *Physica D: Nonlinear Phenomena*, 406:132416, 2020.
- [18] Bernard O Koopman. Hamiltonian systems and transformation in Hilbert space. *Proceedings of the National Academy of Sciences*, 17(5):315, 1931.
- [19] Bernard O. Koopman and John von Neumann. Dynamical systems of continuous spectra. *Proceedings of the National Academy of Sciences*, 18(3):255–263, 1932.
- [20] Milan Korda and Igor Mezić. On convergence of extended dynamic mode decomposition to the koopman operator. *Journal of Nonlinear Science*, 28:687–710, 2018.
- [21] Jonghyeon Lee, Boumediene Hamzi, Boya Hou, Houman Owhadi, Gabriele Santin, and Umesh Vaidya. Kernel methods for the approximation of the eigenfunctions of the koopman operator. *Physica D: Nonlinear Phenomena*, 476:134662, June 2025.
- [22] Bethany Lusch, J Nathan Kutz, and Steven L Brunton. Deep learning for universal linear embeddings of nonlinear dynamics. *Nature communications*, 9(1):4950, 2018.
- [23] Igor Mezić. Spectral properties of dynamical systems, model reduction and decompositions. *Nonlinear Dynamics*, 41:309–325, 2005.
- [24] Igor Mezić. Koopman operator, geometry, and learning. *arXiv: Dynamical Systems*, 2020.
- [25] Wendell H. Mills, Jr. The resolvent stability condition for spectra convergence with application to the finite element approximation of noncompact operators. *SIAM J. Numer. Anal.*, 16(4):695–703, August 1979.

- [26] A. Pazy. *Semigroups of Linear Operators and Applications to Partial Differential Equations*. Applied Mathematical Sciences. Springer New York, 2012.
- [27] Henri Poincaré. Sur le problème des trois corps et les équations de la dynamique. *Acta mathematica*, 13(1):A3–A270, 1890.
- [28] Ali Rahimi and Benjamin Recht. Random features for large-scale kernel machines. *Advances in neural information processing systems*, 20, 2007.
- [29] Itsushi Sakata and Yoshinobu Kawahara. Enhancing spectral analysis in nonlinear dynamics with pseudoeigenfunctions from continuous spectra. *Scientific Reports*, 14(1):19276, 2024.
- [30] Stephen Smale. Differentiable dynamical systems. *Bulletin of the American mathematical Society*, 73(6):747–817, 1967.
- [31] Steven H Strogatz. *Nonlinear dynamics and chaos: with applications to physics, biology, chemistry, and engineering*. Chapman and Hall/CRC, 2024.
- [32] Yoshihiko Susuki, Alexandre Mauroy, and Igor Mezic. Koopman resolvent: A laplace-domain analysis of nonlinear autonomous dynamical systems. *SIAM Journal on Applied Dynamical Systems*, 20(4):2013–2036, 2021.
- [33] Jonathan H Tu. *Dynamic mode decomposition: Theory and applications*. PhD thesis, Princeton University, 2013.
- [34] Matthew O. Williams, Ioannis G. Kevrekidis, and Clarence W. Rowley. A data-driven approximation of the koopman operator: Extending dynamic mode decomposition. *Journal of Nonlinear Science*, 25(6):1307–1346, June 2015.
- [35] M.A. Woodbury and Princeton University. Department of Statistics. *Inverting Modified Matrices*. Memorandum Report / Statistical Research Group, Princeton. Department of Statistics, Princeton University, 1950.
- [36] Yuanchao Xu, Isao Ishikawa, Yuka Hashimoto, and Zhongwei Shen. A data-driven framework for koopman semigroup estimation in stochastic dynamical systems, 2025.
- [37] Yuanchao Xu, Fengyi Li, Masahiro Fujisawa, Xiaoyuan Cheng, Youssef Marzouk, and Isao Ishikawa. Generative modeling through koopman spectral analysis: An operator-theoretic perspective, 2026.